

# 21st Century Change in Global Small-Size Aerosols from Combustion Emissions

Meemong Lee<sup>1</sup>, John Worden<sup>1</sup>, Rebecca Bucholz<sup>2</sup>, Helen Worden<sup>2</sup>, Mijeong Park<sup>2</sup>, Yuan Wang<sup>3</sup>, Jiani Yang<sup>4</sup>, Marcin Witek<sup>5</sup>, Hui Su<sup>1</sup>, Brendan Byrne<sup>6</sup>, Kazu Miyazaki<sup>6</sup>, and Jonathan Jiang<sup>6</sup>

<sup>1</sup>Jet Propulsion Laboratory

<sup>2</sup>National Center for Atmospheric Research, Boulder, CO

<sup>3</sup>California Institute of Technology, Pasadena, CA

<sup>4</sup>California Institute of Technology, Pasadena, CA

<sup>5</sup>Jet propulsion Laboratory, California Institute of Technology, Pasadena, CA

<sup>6</sup>Jet Propulsion Laboratory, California Institute of Technology, Pasadena, CA

November 22, 2022

## Abstract

Changes in aerosol optical depth, both positive and negative, are observed across the globe during the 21st Century. However, attribution of these changes to specific sources is largely uncertain as there are multiple contributing natural and anthropogenic sources that produce aerosols either directly or through secondary chemical reactions. Here we show that satellite-based changes in small-mode AOD between 2002 and 2019 observed in data from MISR can primarily be explained by changes, either directly or indirectly, in combustion emissions. We quantify combustion emissions using MOPITT total column CO observations and the adjoint of the GEOS-Chem global chemistry and transport model. The a priori fire emissions are taken from the Global Fire Emission Data base with small fires (GFED4s) but with fixed a priori for non-fire emissions. Aerosol precursor and direct emissions are updated by re-scaling them with the monthly ratio of the CO posterior to prior emissions. The correlation between modeled and observed AOD improves from a mean of 0.15 to 0.81 for the four industrial regions considered and from 0.52 to 0.75 for the four wildfire-dominant regions considered. Using these updated emissions in the GEOS-Chem global chemistry transport model, our results indicate that surface PM<sub>2.5</sub> have declined across many regions of the globe during the 21st century. For example, PM<sub>2.5</sub> over China has declined by ~30% with smaller fractional declines in E. USA and Europe (from fossil emissions) and in S. America (from fires). These results highlight the importance of forest management and cleaner combustion sources in improving air-quality.

1 **Title: 21<sup>st</sup> Century Changes in Global Small-Size Aerosols from Combustion Emissions**

2 Meemong Lee<sup>1</sup>, John R. Worden<sup>1</sup>, Rebecca Bucholz<sup>2</sup>, Helen Worden<sup>2</sup>, Mijeong Park, Yuan  
3 Wang<sup>3</sup>, Jiani Yang<sup>3</sup>, Marcin Witek<sup>1</sup>, Hui Su<sup>1</sup>, Brendan Byrne<sup>1</sup>, Kazu Miyazaki<sup>1</sup>, Jonathan H.  
4 Jiang<sup>1</sup>

5  
6 <sup>1</sup>Jet Propulsion Laboratory. California Institute for Technology, Pasadena, CA

7 <sup>2</sup>National Center for Atmospheric Research, Boulder, CO

8 <sup>3</sup>Division of Geological and Planetary Sciences, California Institute of Technology, Pasadena,  
9 CA

10 Corresponding author: John Worden ([john.r.worden@jpl.nasa.gov](mailto:john.r.worden@jpl.nasa.gov))

11 ©2021. All rights reserved. California Institute of Technology, government sponsorship  
12 acknowledged

13

14 **Key Points:**

15 Observed changes in small particle AOD in fire prone regions are related to CO emissions and  
16 not CO concentrations.

17

18 Changes in combustion emissions in industrialized countries are correlated with AOD variations.

19

20 Surface PM2.5 as inferred from these changes have declined in many parts of the globe.

21

22 **Plain Language Summary**

23 Aerosols have many different types of sources, e.g. farming, fires, power plants, transportation,  
24 dust, and have large impacts on human health and on climate. We quantify combustion  
25 emissions using satellite observations of carbon monoxide and show that satellite observations of  
26 changes in small particle AOD across the globe are linked to changes in these combustion  
27 sources. These data and model updates indicate substantial declines of PM2.5 (aerosols that  
28 have strong, deleterious effects on human health) across many parts of the globe from changes in  
29 combustion emissions.

30

31  
32  
33  
34  
35  
36  
37  
38  
39  
40  
41  
42  
43  
44  
45  
46  
47  
48  
49  
50  
51

**Abstract** Changes in aerosol optical depth, both positive and negative, are observed across the globe during the 21<sup>st</sup> Century. However, attribution of these changes to specific sources is largely uncertain as there are multiple contributing natural and anthropogenic sources that produce aerosols either directly or through secondary chemical reactions. Here we show that satellite-based changes in small-mode AOD between 2002 and 2019 observed in data from MISR can primarily be explained by changes, either directly or indirectly, in combustion emissions. We quantify combustion emissions using MOPITT total column CO observations and the adjoint of the GEOS-Chem global chemistry and transport model. The *a priori* fire emissions are taken from the Global Fire Emission Data base with small fires (GFED4s) but with fixed *a priori* for non-fire emissions. Aerosol precursor and direct emissions are updated by re-scaling them with the monthly ratio of the CO posterior to prior emissions. The correlation between modeled and observed AOD improves from a mean of 0.15 to 0.81 for the four industrial regions considered and from 0.52 to 0.75 for the four wildfire-dominant regions considered. Using these updated emissions in the GEOS-Chem global chemistry transport model, our results indicate that surface PM<sub>2.5</sub> have declined across many regions of the globe during the 21<sup>st</sup> century. For example, PM<sub>2.5</sub> over China has declined by ~30% with smaller fractional declines in E. USA and Europe (from fossil emissions) and in S. America (from fires). These results highlight the importance of forest management and cleaner combustion sources in improving air-quality.

## 52 **1. Introduction**

53           Aerosols have substantive but contrasting impacts on air-quality and climate. Aerosols can impose  
54 either positive or negative changes in radiative forcing directly by scattering or absorbing sunlight type  
55 (e.g., Sathesh and Ramanathan 2000) or indirectly by changing cloud and rainfall characteristics (e.g.  
56 Andrae *et al.* 2004; Andrae and Rosenfeld 2008; Rosenfeld *et al.* 2014; Jiang *et al.* 2018). These different  
57 effects depend on the aerosol type as well as its source. For example, fires can emit both scattering and  
58 absorbing aerosols with a range of sizes leading to potentially positive or negative impacts on radiative  
59 forcing and rainfall (e.g. Kaufmann *et al.* 2005; Koren *et al.* 2012; Sato *et al.* 2018). Despite these wide-  
60 ranging effects of aerosols on climate it is thought that the direct and indirect effects of aerosols have a net  
61 cooling impact on climate, albeit with uncertainties that are as large as the corresponding radiative forcing

62 estimates, suggesting their net impact is still not well understood (e.g. Seinfeld *et al.* 2016; Fan *et al.* 2016  
63 and refs therein). While this net cooling effect potentially mitigates some of the climate impact from rising  
64 greenhouse gases, an increase in surface aerosols generally leads to poor health outcomes (e.g. Cohen *et*  
65 *al.* 2015 and refs therein). Understanding the location of aerosol emissions and their types is therefore  
66 critical towards understanding global climate and health outcomes as a consequence of anthropogenic  
67 activities and changes.

68 Previous studies using satellite and ground-based data have shown significant changes in the  
69 aerosol burden during the 21st century in many industrialized regions (e.g., Donkelaar *et al.* 2015; Mheta *et*  
70 *al.* 2016; Zhao *et al.* 2017). For example, the eastern USA and western Europe show declines in aerosol  
71 loading whereas China shows a strong increase in the early 21st century followed by a decrease in the  
72 second decade (Wang *et al.* 2015). In contrast, India shows a steady increase in aerosol loading (Dey and  
73 Girolamo 2011; Zhao *et al.* 2017). While the causes of these changes are likely related to human activities  
74 the exact attribution is uncertain as agriculture, construction, biomass burning, the automobile and energy  
75 sector all contribute significantly to dust and aerosols either directly or indirectly through emission of aerosol  
76 pre-cursors and subsequent chemical transformation. Natural sources of aerosols such as biogenic  
77 secondary organic aerosols, sea salt, and mineral dust also contribute substantively to the overall aerosol  
78 burden (e.g. Jaegle *et al.* 2011; Mahowald 2011; Rosenfeld *et al.* 2014; Bauer *et al.* 2019). In this  
79 manuscript we focus on attribution of small-mode aerosols as measured by the Multi-angle Imaging  
80 Spectroradiometer (MISR) (e.g., Ragray *et al.* 2010 and refs therein) as these are primarily associated with  
81 aerosols from combustion sources and contribute significantly to surface PM<sub>2.5</sub> (e.g. Eck *et al.* 2010).  
82 Figure 1 (top left) shows the total AOD for small-mode particles from the MISR instrument. As seen in  
83 Figure 1, Central Africa is one of the largest sources of small-mode aerosols and is likely related to biomass  
84 burning and dust (e.g., Roberts *et al.* 2001). Direct emission from combustion sources, as well as secondary  
85 aerosol formation from ammonia and sulfates are the largest sources of aerosols in East Asia (e.g., Huang *et*  
86 *al.* 2014). Over India (e.g. Ramanathan *et al.* 2001; 2005) large sources of aerosols are related to agriculture,  
87 transport, coal plants, biomass and biofuel burning, and construction. Similarly, direct and secondary  
88 aerosol sources in the USA are likely related to energy, transportation, and agricultural sectors (e.g., Liao *et*  
89 *al.* 2007; Burney 2020).

90 Observed changes in the small-mode AOD (from MISR) are shown in the bottom left panel of Figure  
91 1. These changes are consistent with observations of aerosols using multiple satellite and ground  
92 measurements in the industrial regions of North America, Europe, India, and Asia with the largest changes

93 in India and Asia but also in South America and smaller but observable changes in the Eastern USA  
94 Western Europe, Africa and Australia (e.g. Buchholz *et al.* 2020). These regions have also seen substantive  
95 changes in combustion emissions and aerosol pre-cursors as found by satellite observations of trace gasses  
96 such as CO, NH<sub>3</sub>, SO<sub>2</sub>, and NO<sub>2</sub> (e.g., Jiang *et al.* 2015; Yin *et al.* 2015; Warner *et al.* 2015; Hilboll *et al.*  
97 2013; Krotkov *et al.* 2016; Jiang *et al.* 2017). Recently, Buchholz *et al.* (2021) examined multi-decadal  
98 trends in both AOD and CO abundance from the NASA Terra Moderate resolution Imaging Spectrometer  
99 (MODIS) and Measurements of Pollution in the Troposphere (MOPITT) satellite instruments respectively  
100 and found significant spatial and temporal correlations in regions with high biomass burning activity,  
101 suggesting a causal link between CO (a tracer for combustion) and AOD. However, CO and aerosols have  
102 different photochemical lifetimes leading to seasonal cycles in abundance that are often out of phase in  
103 industrial regions, which complicate the attribution of the relationship between these atmospheric species.  
104 Therefore, in this research we quantify global CO emissions using almost two decades of satellite  
105 observations integrated into a global chemistry transport model to determine to what extent decadal changes  
106 in combustion emissions can explain changes in small-mode aerosols and corresponding optical depth.  
107

## 108 **2. Change in Combustion Emissions and Corresponding Small-mode AOD**

109 Atmospheric carbon monoxide (CO) is a product of the oxidation of atmospheric hydrocarbons and  
110 non-methane volatile organic carbons and is also emitted during burning of fossil fuels as a result of  
111 incomplete combustion. CO emissions have been quantified from a variety of aircraft and satellite data  
112 using global and regional chemistry transport models and different inversion approaches for relating  
113 observed concentrations to emissions (e.g. Jiang *et al.* 2015; Yin *et al.* 2015 and refs therein).

114 Here we quantify CO emissions using version 8 multispectral total column CO observations from the  
115 NASA Terra MOPITT instrument (e.g. , Deeter *et al.* 2019) and a 4D variational adjoint approach based on  
116 the GEOS-Chem global chemical transport model (Henze *et al.* 2007, Appendices 1 and 2). The approach  
117 we use is similar to and builds from previous work described in Jiang *et al.* (2017) and Worden *et al.* (2017)  
118 which also quantified CO emissions and used them for evaluating decadal changes in fire emissions of CH<sub>4</sub>  
119 and CO. Yearly, *a priori* for the fire emissions are from the GFED4s (van der Werf *et al.*, 2017) data  
120 base and span the time series shown in the figure. All other combustion emissions for the *a priori* are fixed  
121 as they are from a combination of sources that do not span the time period shown (Table A2).

122 The upper right panel of Figure 1 shows the change in CO emissions for the time period corresponding  
123 to the observed changes in AOD in the bottom left panel. These results are consistent with previous studies  
124 using the MOPITT CO record (Jiang *et al.* 2015; Yin *et al.* 2015). As seen by visually comparing the top  
125 right and bottom left panel of Figure 1, many of the changes in CO emissions are found to be of the same  
126 sign and in the same regions as changes in MISR small-mode AOD.

127 In order to determine to what extent changes in small-mode AOD are related to changes in CO  
128 emissions we first update the primary aerosol emission precursors (Tables A2 and A3) by multiplying their  
129 emissions at each grid box by the ratio of the posterior to prior CO emissions. Aerosols (and AOD) are then  
130 computed either directly from the emissions or through secondary aerosol formation within the GEOS-  
131 Chem model. While we can attribute CO emissions to fires with this approach because most biomass  
132 burning has distinct seasonality and is straightforward to identify using other metrics such as burned area,  
133 we cannot unequivocally partition CO emissions into other combustion sources such as the energy and  
134 transport sector or to biogenic sources using this approach. However, previous studies indicate that the CO  
135 emissions in most industrialized countries are related to burning of fossil fuels and that biogenic emissions  
136 and oxidation of atmospheric hydrocarbons do not vary as much as the other sources (e.g. Jiang *et al.* 2015;  
137 H. Worden *et al.* 2019). This approach assumes that aerosols are tied either directly to combustion  
138 emissions such as through a change to cleaner burning, more efficient fuels, or that their changes are  
139 indirectly related by, for example, co-temporaneous policy directives that reduces aerosols while increasing  
140 combustion efficiency, or alternatively through changes in activity. The model AOD accounts for the  
141 column-wise integration of the MISR instrument and the sample time of the sun-synchronous orbit  
142 (Appendix-3). The modeled change in small-mode AOD is shown in the bottom right panel of Figure 1.  
143 Visual inspection confirms similar changes in both observed and modeled small-mode AOD in many of the  
144 high-emitting areas (labeled in bottom right panel).

145 We next compare in more detail the mean estimates of small-mode AOD and corresponding  
146 observations in Figures 2 and 3 for the regions labeled in Figure 1 (bottom right panel). Figure 2 shows a  
147 comparison for the industrial regions of the USA, Europe, India, and China between the modeled and  
148 observed small-mode AOD changes depicted in Figure 1. These comparisons show that observed and  
149 modeled trends are consistent within the uncertainties for the USA, Europe, and China and that the direct  
150 emission of small-mode aerosols from combustion explains the interannual to decadal changes in these  
151 aerosols. However, CO emissions and corresponding small-mode AOD over India do not show much of a  
152 trend, likely because of challenges in quantifying emissions in this region due to complexities in

153 atmospheric transport (e.g., Worden *et al.* 2010; Liu *et al.* 2010; Jiang *et al.* 2013; Jiang *et al.* 2015). In  
154 addition, the posterior emissions better capture the decadal variability relative to the prior as shown in Table  
155 1. For example, the MISR observed small-mode AOD difference between the two decades for E. China is -  
156  $0.031 \pm 0.022$ , in agreement with the updated modeled emissions difference of  $-0.038 \pm 0.0018$ .

157 Figure 3 shows a comparison of modeled small-mode AOD from fires against MISR observed small-  
158 mode AOD in regions that have high biomass burning as indicated by burned area. These comparisons are  
159 again consistent between the model and observation within the uncertainty levels. We find that small-mode  
160 AOD based on CO emissions shows substantial improvement in the inter-annual variability (IAV) as  
161 demonstrated by the improved correlations. Notably, the decadal changes in small-mode AOD are  
162 consistent with previous observations of a decline in fires in S. America and Indonesia (e.g., Andela *et al.*  
163 2017, Worden *et al.* 2017). Table 1 also shows the decadal differences for the regions dominated by fire  
164 emissions. In contrast to the improved agreement in IAV found for the anthropogenic regions where the  
165 prior emission is fixed, there is not much improvement in these comparisons where the prior emission is  
166 annually set, likely because the trends in burned area are similar to prior CO emissions in these regions  
167 (Worden *et al.* 2017).

168 We next test if changes in meteorology can also explain the small-mode AOD variability by performing  
169 a model run with fixed emissions (Appendix 4) and find that changes in dynamics cannot explain the  
170 observed variability in small-mode AOD. Variations in biogenic emissions may play a role in tropical  
171 regions, however these variations are small relative to variations in biomass burning in these same regions  
172 (Jiang *et al.* 2015; H. Worden *et al.* 2019). Other confounding factors are the large uncertainties in aerosol  
173 formation, the partitioning of these sources and how both combustion and non-combustion sources affect  
174 AOD. Uncertainties from these other factors cannot be easily calculated due to computational challenges  
175 and poor knowledge about their uncertainty characteristics. Hence our result that for the non-fire sector that  
176 small-mode AOD is correlated with CO emissions should be taken as purely empirical with additional  
177 analysis needed to relate observed variability to specific emissions.

178

### 179 **3. Discussion and Implications**

180 Decreasing both aerosol and CO emissions can be accomplished in multiple ways, both directly and  
181 indirectly, and need not be causally related. We expect a concurrent change in CO emissions and small-  
182 mode AOD for fire emissions as both are released during combustion (e.g., van der Werf 2010, 2017;

183 Worden *et al.* 2017; Andela *et al.* 2017). A switch from coal to natural gas also results in both reduced  
184 aerosols and improved combustion efficiency resulting in lower CO emissions (e.g., Burney 2020,  
185 Buchholz *et al.*, 2021); however, we do not attempt to estimate how much of the observed change in small-  
186 mode AOD across the globe is due to this coal-to-gas fuel transition and leave this to a subsequent study. On  
187 the other hand, policies implemented contemporaneously that result in improved filtering of aerosols and  
188 increased combustion efficiency such as for from coal-powered plants (Karplus *et al.* 2017; Lu *et al.* 2020)  
189 and other combustion sources such as from traffic can result in the same outcome of reduced AOD and CO  
190 emissions. Changes in agricultural CO and aerosol emissions may also be correlated entirely through  
191 activity (Warner *et al.* 2017) as aerosol pre-cursors from fertilizer use, as well as the corresponding dust and  
192 combustion associated with farming can occur in tandem. Nonetheless, the empirical observation shown  
193 here that changes in small-mode AOD are well correlated with changes in CO emissions in N. America,  
194 Europe, and Asia suggest a link between the two that should be tested in subsequent studies; this would  
195 require more in-depth analysis between the different emission sectors and aerosol emissions. We note that  
196 these changes in emission do not necessarily reflect a decrease or increase in carbon dioxide except in fire-  
197 prone regions but instead reflects a change in combustion efficiency as overall CO<sub>2</sub> levels continue to  
198 increase during this time period (Friedlingstein *et al.* 2019).

199 The decline in observed small-mode AOD in N. America, Europe, China, and S. America has  
200 implications for air quality in these regions as they are correlated with near-surface aerosols and  
201 subsequently with PM 2.5 concentrations (e.g., Donkelaar *et al.* 2015). To quantify these effects, we show  
202 (Figure 4) the modeled surface PM2.5 concentrations and its changes that correspond to aerosol and CO  
203 emission changes shown in Figures 1 through 3. The top left panel of Figure 4 shows the mean PM2.5  
204 concentration from all sources based on the GEOS-Chem model. Largest values of PM2.5 concentrations  
205 from are in desert regions and are due to fine-mode mineral dust (e.g., Bauer *et al.* 2019). The top right panel  
206 shows the net change in PM2.5 globally whereas the bottom panels show the changes for the industrial  
207 (bottom left) and fire prone (bottom right) regions. The sign of these changes is consistent with a number of  
208 local and regional studies using ground-based data. The biggest improvement in the magnitude of PM2.5 is  
209 in China, consistent with Lu *et al.* (2020 and refs therein) with smaller changes in the magnitude of PM2.5  
210 in N. America (e.g. Bennett *et al.* 2019). The decline of PM2.5 in Europe and slight increase in E. Australia  
211 are consistent with observed changes in PM2.5 in corresponding urban locations (e.g. de Jesus *et al.* 2020).  
212 The increase in Indonesia is driven almost entirely by the 2015 ENSO related fires but if these are removed  
213 there is a small decrease. Exact comparisons between these model based (but data constrained) estimates of

214 surface PM2.5 decadal changes and local surface measurements are challenging because of the difference in  
215 scales between the measurements. Nonetheless, these results indicate that a reduction in combustion related  
216 air-quality emissions in these areas have improved the air quality. However, the climate impacts of these  
217 changes are uncertain as this study is not able to determine if there has been a shift from sulfate aerosols,  
218 which mainly scatter radiation, to black carbon aerosols, which also absorbs radiation. A shift to black  
219 carbon, even as aerosols are reduced, could have negative climate impact due to the increased atmospheric  
220 heating even if there is a reduced radiation transferred to the surface (e.g. Haywood and Ramaswamy 1998;  
221 Ramanathan et al. 2001, 2005, Streets *et al.* 2006 and refs therein).

222

### 223 **Acknowledgements**

224 This research was carried out at the Jet Propulsion Laboratory, California Institute of Technology  
225 under a contract with National Aeronautics and Space Administration (80NM0018D0004). We  
226 acknowledge the funding support by the JPL Strategic Advances in Air Quality Research and  
227 Technology Development. We also thank the support from NASA ROSES ACPMAP and  
228 TASNPP programs. ©2021. All rights reserved.

### 229 **Data Statement**

230 The satellite data used in this study are publicly available for download at NASA website  
231 <https://earthdata.nasa.gov/about/daacs>. In addition, websites available for data download include:  
232 MOPITT level 2 data products: <ftp://15ft101.larc.nasa.gov/MOPITT/MOP02J.008>; MISR level 2  
233 data products: <ftp://15ft101.larc.nasa.gov/MISR>. All data underlying this article are available in  
234 the article. For additional questions regarding the data sharing and data assimilation system,  
235 please contact the corresponding author at [John.R.Worden@jpl.nasa.gov](mailto:John.R.Worden@jpl.nasa.gov).

236

### 237 **Author contributions**

238 J.W., M.L., and J.J. designed the research; M. L performed the CO flux inversion, AOD model  
239 simulation, and comparison of the modeled AOD with the MISR-AOD. J.W and M.L wrote the  
240 manuscript and the co-authors assisted in manuscript preparation. Several co-authors are also  
241 involved in evaluating the results and preparing the data needed for this research. These include  
242 B.B. for ATom CO comparison, M. W. for MISR AOD mode properties, and K. M. for OH,  
243 SO<sub>2</sub>, and NO<sub>x</sub> data products.

244

245 **Appendix**

246

247 ***A.1 GEOS-Chem emission inventories.***

248 We organize emission inventories for CO and aerosols integrating anthropogenic, biofuel,  
249 biogenic, and fire emission sources. For the non-fire emission sources, a combination of global  
250 and regional emission inventories are used in this study (Table A2). The global models include  
251 EDGAR (Olivier and Berdowski, 2001), Global Emission Initiative (GEIA) (A.F. Bouwman,  
252 1997), and Bond (T.C. Bond et al 2007). The regional models include the US Environmental  
253 Protection Agency (EPA) National Emission Inventory (NEI) for 2008 in North America, the  
254 Criteria Air Contaminants (CAC) inventory for Canada, the Big Bend Regional Aerosol and  
255 Visibility Observational (BRAVO) Study Emissions Inventory for Mexico (Kuhns et al.,2003),  
256 the Cooperative Program for Monitoring and Evaluation of the Long-range Transmission of Air  
257 Pollutants in Europe (EMEP) inventory for Europe in 2000 (Vestreng and Klein, 2002) and the  
258 Streets Asia emissions inventory for 2000. For the biogenic emission type, we employ the Model  
259 of Emissions of Gases and Aerosols from Nature, version2.1 (MEGAN; Guenther et al., 2012)  
260 and MERRA 2 meteorology to derive CO and OC emissions and integrate the off-line emission  
261 inventory from GEIA for NH3. For fire emission, we derive emissions for the above five  
262 constituents based on the dry mass GFED4s (van der Werf et al., 2017).

263 We prepare the non-fire emission inventories only for a single year due to limited temporal  
264 coverage of the emission datasets described above. For the fire emission, we prepare a single  
265 year inventory for the first decade (2002-2009) but annual inventories for the second decade. All  
266 emission datasets are at 2°x2.5° spatial resolution with 3 hourly temporal resolution. The total  
267 emission budget integrating the non-fire and the fire emissions are shown for different regions in  
268 Table A2.

269

270 ***A.2 Adjoint model based 4DVAR Assimilation Process.***

271 We use the Greenhouse Gas Framework – Flux (GHGF-Flux) 4D-Var assimilation system  
272 for CO flux inversions. This system has been developed under the NASA Carbon Monitoring  
273 System (CMS) project and inherits the chemistry transport model and adjoint model from the

274 GEOS-Chem adjoint (Liu et al., 2020; Byrne et al., 2020). We drive the chemical transport by  
275 the Modern-Era Retrospective Analysis for Research and Applications, Version 2 (MERRA-2)  
276 meteorology products. For OH field, we combine the tropospheric-OH data products obtained  
277 from the TCR-2 framework (Miyazaki et al., 2020) and the stratospheric OH data products from  
278 the Global Modeling Initiative (GMI, <https://gmi.gsfx.nasa.gov>) of the NASA Modeling  
279 Analysis and Prediction Program.

280 The 4D-Var data assimilation system minimizes a cost function which is defined as

281

$$282 \quad J(\mathbf{x}) = \sum_{i=1,N} (\mathbf{F}_i(\mathbf{x}) - \mathbf{y}_i)^T \mathbf{R}^{-1} (\mathbf{F}_i(\mathbf{x}) - \mathbf{y}_i) + (\mathbf{x} - \mathbf{x}_a)^T \mathbf{B}^{-1} (\mathbf{x} - \mathbf{x}_a)$$

283

284 where  $\mathbf{x}$  is the state vector of CO emission,  $N$  is the number of observations within the  
285 assimilation period,  $\mathbf{y}$  is the observed state,  $\mathbf{F}(\mathbf{x})$  is the forward model, and  $\mathbf{R}$  and  $\mathbf{B}$  are variance  
286 of the observed state and the prior CO emission. We optimize a scaling factor array applied to  
287 the prior CO emission with the assimilation window of one month. We sequentially perform the  
288 monthly assimilation process generating the initial condition of the succeeding month based on  
289 the optimized CO emission. For the assimilation process, we organize prior CO emissions  
290 integrating emissions from anthropogenic, biogenic, and fire emission sources.

291 To evaluate the fidelity of the CO emission estimates, we compare the prior and the posterior  
292 CO concentrations against in-situ CO measurements. Figure 5 and 6 show the comparison  
293 against the surface flask measurements and the NASA's Atmospheric Tomography Mission  
294 (ATOM). The surface flask measurements are typically over continental regions whereas the  
295 ATOM data are typically over the ocean. Both sets of comparisons show improvement between  
296 prior and posterior as compared to these data sets.

297

### 298 ***A.3 Aerosol Emission Inventories and AOD Change Estimation.***

299 The AOD is a function of the aerosol concentration and the particle properties of the aerosol  
300 type. We simulate AOD and the surface PM<sub>2.5</sub> from sulfate aerosols and carbonaceous aerosols  
301 to compare with the small mode MISR-AOD. In GEOS-Chem, the sulfate aerosol tracers include  
302 SO<sub>4</sub>, ammonia (NH<sub>4</sub>), and Nitrate (NIT) and the carbonaceous aerosol tracers include hydrophilic  
303 black carbon (BCPI), hydrophobic black carbon (BCPO), hydrophilic organic carbon (OCPI),  
304 and hydrophobic organic carbon (OCPO). The SO<sub>4</sub> emission is derived as a fraction of the SO<sub>2</sub>

305 emission, 3% globally, 5% over USA, and 1.3 % over Europe and the BC and OC emissions are  
306 shared between the hydrophobic and hydrophilic carbonaceous aerosols, 20 % and 80%,  
307 respectively. The gas-to-particle reactions of the sulfate aerosols (Metzger et al, 2002) involve  
308 SO<sub>4</sub>, NH<sub>3</sub>, and HNO<sub>3</sub>. We integrate the tropospheric-NO<sub>x</sub> emissions from the TCR-2 framework  
309 for HNO<sub>3</sub> concentration simulation.

310 To estimate the AOD changes due to the combustion emissions, we update the prior aerosol  
311 emissions of BC, OC, and SO<sub>2</sub> (Appendix 1) with the optimal emission scale factors obtained  
312 from the MOPITT-CO assimilation (Appendix 2). The posterior aerosol emissions (i.e., updated  
313 prior aerosol emissions) provide a full coverage between 2002 and 2019 for the anthropogenic,  
314 biofuel, and biogenic emission types following the posterior CO emission trend. The fire  
315 emissions for BC, OC, SO<sub>2</sub>, and NH<sub>3</sub> are computed based on the updated dry mass and the  
316 corresponding emission factors. Note that the posterior NH<sub>3</sub> emission is updated only for the fire  
317 emission type, consequently changes in agriculture and livestock which also affect NH<sub>3</sub>  
318 emissions (Warner *et al.* 2017; van Damme *et al.* 2018) are not included in the estimated AOD  
319 changes shown in Figure 1. Table A4 lists the decadal mean (average of the annual mean over a  
320 decade) of the posterior emission inventories of CO, BC, OC, SO<sub>2</sub>, and NH<sub>3</sub>.

321

#### 322 ***A.4 AOD variations for constant emission scenario***

323 Variations in wind fields, humidity, and temperature all affect aerosol emission and  
324 subsequent AOD; in this study we test if changes in these environmental parameters can also  
325 explain changes to the observed AOD. The atmospheric dynamics model simulation requires the  
326 surface pressure, temperature, winds, planetary boundary layer height, cloud mass flux, and  
327 detrainment. The wet scavenging model simulation requires the relative humidity, precipitation,  
328 and rain water source. The dry deposition model simulation requires the surface temperature, the  
329 surface roughness, and the albedo. To test whether decadal variations in meteorology can explain  
330 observed small-mode AOD trends we run the AOD model simulation for the entire study time  
331 period keeping the emissions constant and changing only the meteorology fields. Figure 7 shows  
332 the results of this study and demonstrates the changes in environmental factors cannot explain  
333 observed decadal changes in AOD as AOD remains approximately constant for all regions for  
334 this scenario.

335

336  
 337  
 338  
 339

**Table 1 Decadal trend of the MISR AOD, Prior AOD, and Posterior AOD**

Region	AOD	Decade 1 (2002-2010)	Decade 2 (2011-2019)	Change (Decade2 – Decade1)
E China	MISR	0.19656 ± 0.00892	0.16575 ± 0.02093	-0.03081 ± 0.02275
	Prior	0.17979 ± 0.00429	0.17884 ± 0.00461	-0.00094 ± 0.00630
	Posterior	0.19315 ± 0.00935	0.15547 ± 0.01541	-0.03768 ± 0.01802
Europe	MISR	0.06031 ± 0.00506	0.05002 ± 0.00454	-0.01029 ± 0.00680
	Prior	0.05535 ± 0.00158	0.05530 ± 0.00173	-0.00006 ± 0.00234
	Posterior	0.05939 ± 0.00640	0.05239 ± 0.00285	-0.00700 ± 0.00700
India	MISR	0.13437 ± 0.00684	0.15358 ± 0.00648	0.01922 ± 0.00943
	Prior	0.09298 ± 0.00279	0.09168 ± 0.00183	-0.00130 ± 0.00333
	Posterior	0.08698 ± 0.00886	0.09201 ± 0.00357	0.00503 ± 0.00955
USA-East	MISR	0.08291 ± 0.00759	0.06393 ± 0.00882	-0.01898 ± 0.01164
	Prior	0.07511 ± 0.00182	0.07669 ± 0.00202	0.00158 ± 0.00272
	Posterior	0.07523 ± 0.00585	0.07061 ± 0.00653	-0.00462 ± 0.00877
Africa	MISR	0.14092 ± 0.00615	0.14544 ± 0.00502	0.00452 ± 0.00794
	Prior	0.11285 ± 0.00435	0.11669 ± 0.00355	0.00384 ± 0.00561
	Posterior	0.12460 ± 0.00687	0.12664 ± 0.00606	0.00204 ± 0.00916
Australia	MISR	0.04148 ± 0.00358	0.04336 ± 0.00355	0.00188 ± 0.00504
	Prior	0.02831 ± 0.00230	0.02807 ± 0.00339	-0.00024 ± 0.00410
	Posterior	0.04472 ± 0.00433	0.04241 ± 0.00592	-0.00231 ± 0.00733
Indonesia	MISR	0.06775 ± 0.01481	0.06894 ± 0.01853	0.00119 ± 0.02372
	Prior	0.04470 ± 0.00400	0.05689 ± 0.01662	0.01219 ± 0.01710
	Posterior	0.05695 ± 0.01427	0.06101 ± 0.02926	0.00406 ± 0.03256
S. America	MISR	0.07900 ± 0.01169	0.06838 ± 0.00894	-0.01062 ± 0.01472
	Prior	0.06406 ± 0.00859	0.05719 ± 0.00567	-0.00686 ± 0.01029
	Posterior	0.07288 ± 0.01077	0.05460 ± 0.00764	-0.01828 ± 0.01321

340  
 341  
 342  
 343  
 344  
 345  
 346

Table 1 lists the mean and variance of small mode MISR AOD, the model AOD computed with the prior aerosol emissions (prior), and the model AOD computed with the updated aerosol emissions by the ratio of the CO posterior to prior emission (posterior) for two decades. The change column shows the mean value change between the two decades with the uncertainty computed as the root mean square of the respective variances.

347  
348  
349

**Table A2 Prior Emission Inventory Organization**

Emission type	Emission model	CO Tg CO /year	BC Tg C /year	OC Tg C /year	SO <sub>2</sub> Tg SO <sub>2</sub> /year	NH <sub>3</sub> Tg NH <sub>3</sub> /year
Anthropogenic	EDGAR + regional	470 (0.37)			29.69 (0.95)	32.51 (0.64)
	Bond		2.98 (0.49)	3.05 (0.10)		
Biofuel	GEIA	232 (0.18)			0.27 (0.01)	1.61 (0.03)
	Bond		1.55 (0.26)	6.28 (0.20)		
Biogenic	MEGAN	235 (0.18)	0.0	8.97 (0.29)	0.0	
	GEIA					14.26 (0.28)
Fire (mean)	GFED4	333 (0.26)	1.53 (0.25)	12.86 (0.41)	0.96 (0.03)	2.67 (0.05)
Total		1270 (1.00)	6.05 (1.00)	31.17 (1.00)	30.92 (1.00)	51.05 (1.00)

350  
351 Table A2 lists the emissions from the prior emission inventories for CO, BC, OC, SO<sub>2</sub>, and NH<sub>3</sub>  
352 with respect to four emission types (anthropogenic, biofuel, biogenic, and fire) and the  
353 contribution (fraction) of each emission type to the total emission budget in parentheses. The  
354 emission models within each emission type represent the provenance of the emission data  
355 products or derivation processes (e.g., MEGAN and GFED4).

356  
357  
358  
359  
360  
361

362

363

364

**Table A3 Global and Regional Annual Budget of Prior Emissions**

	<b>CO</b> (TgCO /year)	<b>BC</b> (Tg C/year)	<b>OC</b> (Tg C/year)	<b>SO<sub>2</sub></b> (Tg SO <sub>2</sub> /year)	<b>NH<sub>3</sub></b> (Tg NH <sub>3</sub> /year)
Global	1270	6.05	31.17	30.92	51.05
Anthropogenic regions					
USA-east	35.51	0.17	0.49	2.95	1.15
Europe	27.90	0.32	0.50	1.45	2.92
India	115.53	0.49	1.57	1.57	6.29
China	152.53	0.98	2.00	6.20	4.74
Fire regions					
Africa	164.86	0.80	6.02	0.84	2.68
Indonesia	78.23	0.23	1.77	1.65	1.35
S. America	140.63	0.33	3.85	2.21	2.89
Australia	32.78	0.11	0.99	1.30	0.99

365

366 Table A3 lists the global emission budget (Total emission in Table A2) and regional distribution

367 in the four anthropogenic regions and the four fire regions shown in Figure 1.d.

368

369

370

371

372

373

374

375

376

377

378

379

380

381

382

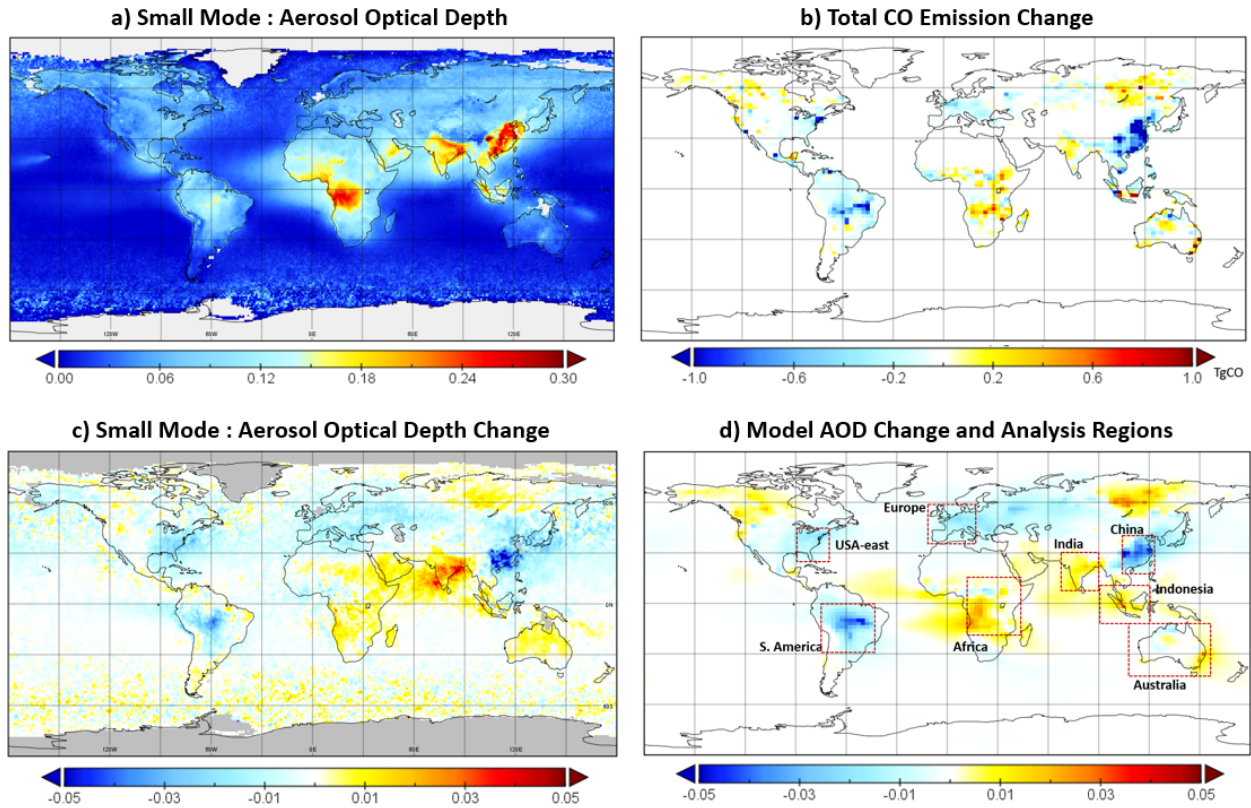
383

**Table A4 Decadal Comparison of Posterior Emissions**

	<b>CO</b> (Tg CO/year)		<b>BC</b> (Tg C/year)		<b>OC</b> (Tg C/year)		<b>SO<sub>2</sub></b> (Tg SO <sub>2</sub> /year)		<b>NH<sub>3</sub></b> (Tg NH <sub>3</sub> /year)	
	1	2	1	2	1	2	1	2	1	2
Decade	1	2	1	2	1	2	1	2	1	2
globe	1592	1465	8.02	7.30	37.61	36.30	42.88	36.41	51.05	50.72
Anthropogenic regions										
USA-east	56	47	0.33	0.27	0.91	0.78	5.9	4.50	1.15	1.15
Europe	52	45	0.61	0.52	0.95	0.84	2.44	2.16	2.92	2.92
India	92	93	0.42	0.42	1.33	1.32	1.45	1.47	5.46	5.46
China	149	113	1.11	0.84	2.23	1.68	6.86	5.18	4.86	4.86
Fire regions										
Africa	179	189	0.87	0.93	6.38	6.77	0.99	1.08	3.77	3.99
Indonesia	55	52	0.24	0.21	1.51	1.51	1.86	1.57	1.42	1.25
S. America	153	121	0.43	0.33	4.03	3.13	2.37	2.27	3.46	3.12
Australia	63	67	0.23	0.22	1.87	2.08	1.99	1.99	1.54	1.56

384

385 Table A4 compares the average annual budget of the posterior emissions of CO, BC, OC, SO<sub>2</sub>,  
386 and NH<sub>3</sub> between the first decade (2002-2009) and the second decade (2010-2019), globally and  
387 regionally. Note that the NH<sub>3</sub> posterior emission is updated only for the fire emission type.

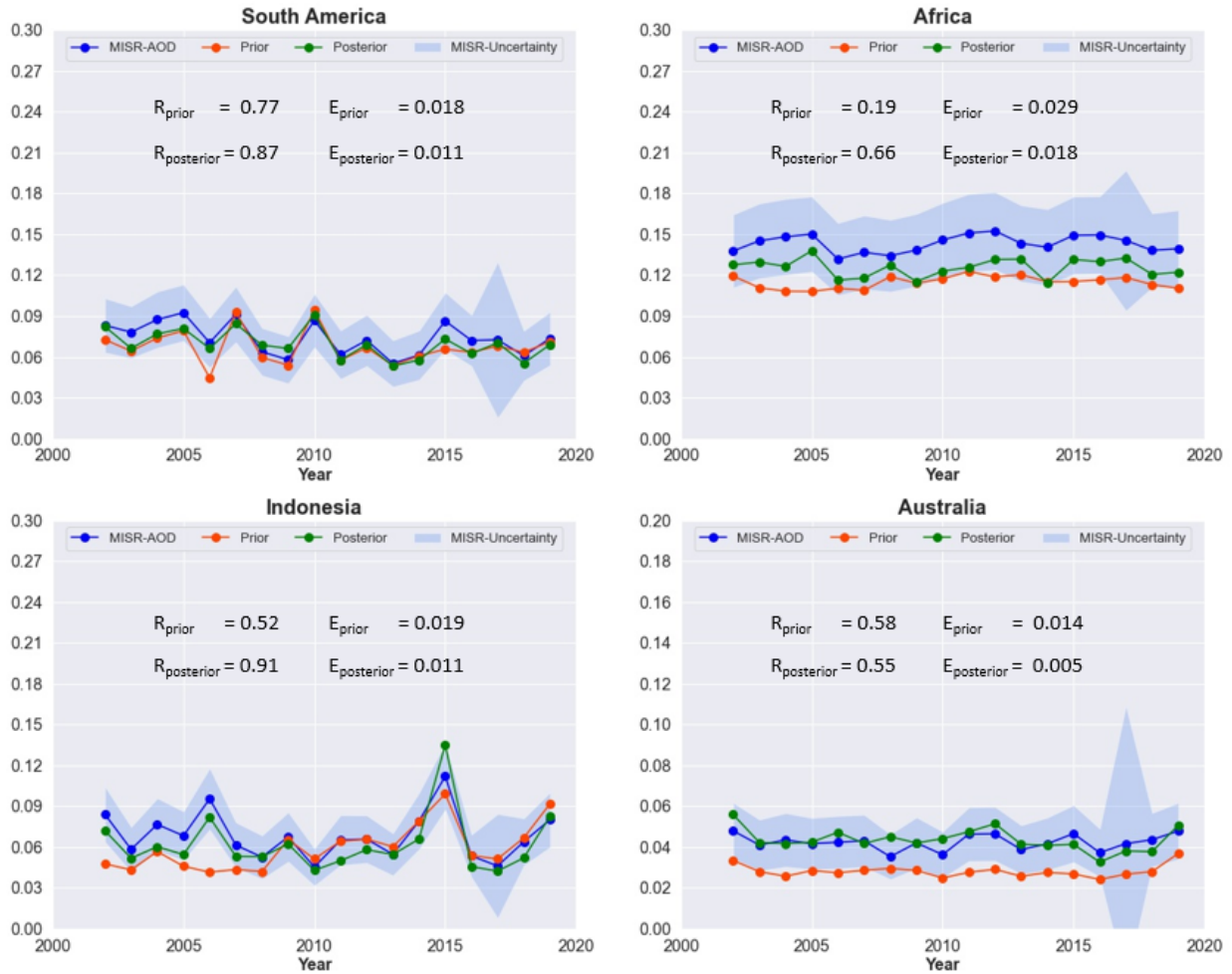


388  
 389 **Figure 1.** Relationships between combustion emissions and AOD of the small size aerosols (<  
 390 0.7  $\mu\text{m}$  in diameter) during the two decades (2002-2019): (a) average of the annual mean AOD  
 391 over two decades of the small-mode MISR-AOD, (b) decadal change of the total CO emission  
 392 annual budget, (c) decadal change of the small-mode MISR-AOD, and (d) decadal change of the  
 393 model-AOD with an overlay of the eight study regions, where the decadal change refers to the  
 394 average of the annual mean over the second decade minus the average of the annual mean over  
 395 the first decade. Figure 1.d overlays the eight study regions selected for the annual trend  
 396 investigation, four regions with a high level of anthropogenic pollution (China, India, Europe,  
 397 and eastern USA) and four regions with a high level of wild-fire events (South America, Africa,  
 398 Indonesia, and Australia).  
 399



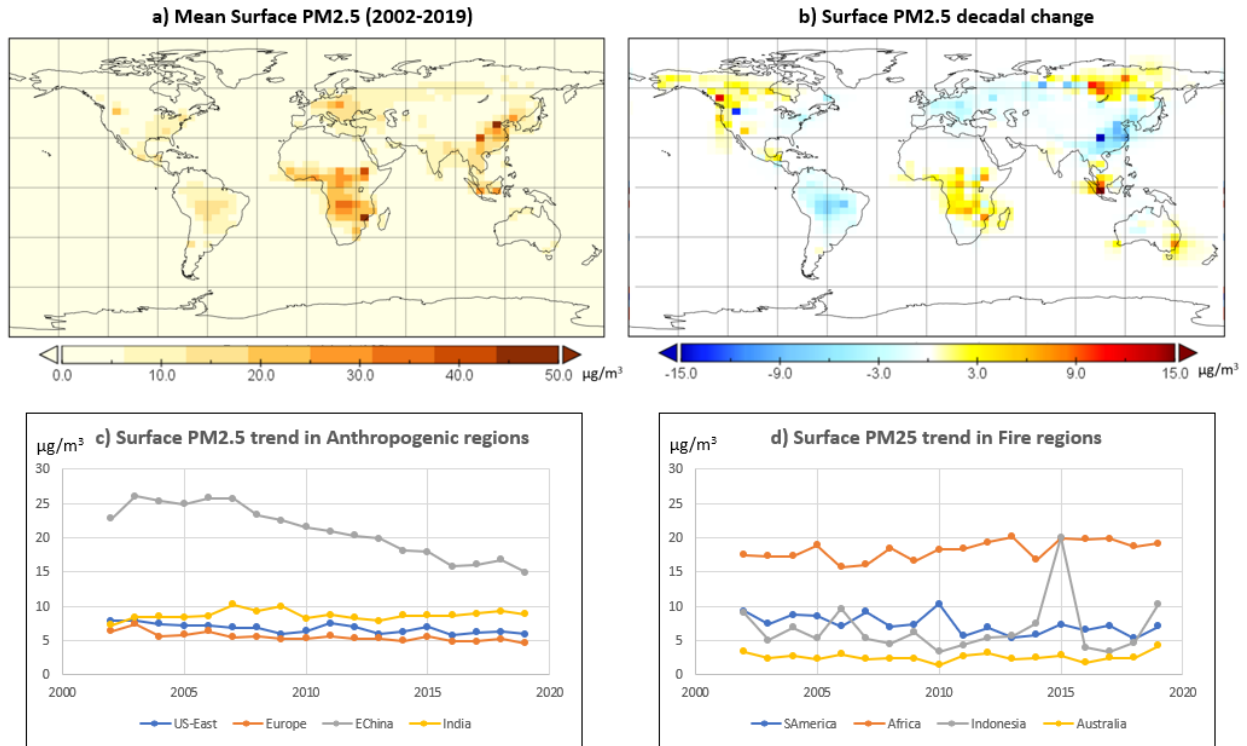
400  
 401 **Figure 2.** Comparison of small-mode MISR AOD, model AOD computed with the prior aerosol  
 402 emission (prior), and model AOD computed with the posterior aerosol emission (posterior) in  
 403 four anthropogenic regions (Figure 1.d). The R value represent the correlation between the  
 404 model AOD and the small-mode MISR-AOD and the E value are the root mean square  
 405 difference between the model AOD and the small-mode MISR-AOD.

406  
 407

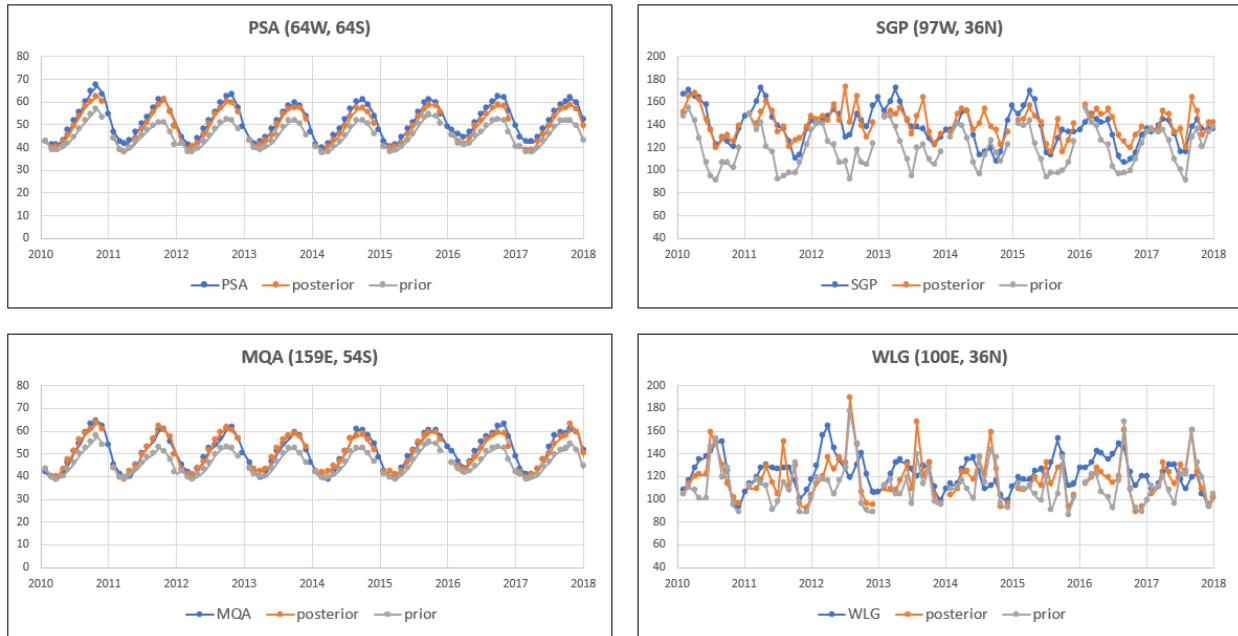


408  
 409 **Figure 3.** Comparison of small-mode MISR AOD, model AOD computed with the prior aerosol  
 410 emission (prior), and model AOD computed with the posterior aerosol emission (posterior) in  
 411 four wildfire dominant regions (Figure 1.d). The R value represent the correlation between the  
 412 model AOD and the small-mode MISR-AOD and the E value are the root mean square  
 413 difference between the model AOD and the small-mode MISR-AOD.

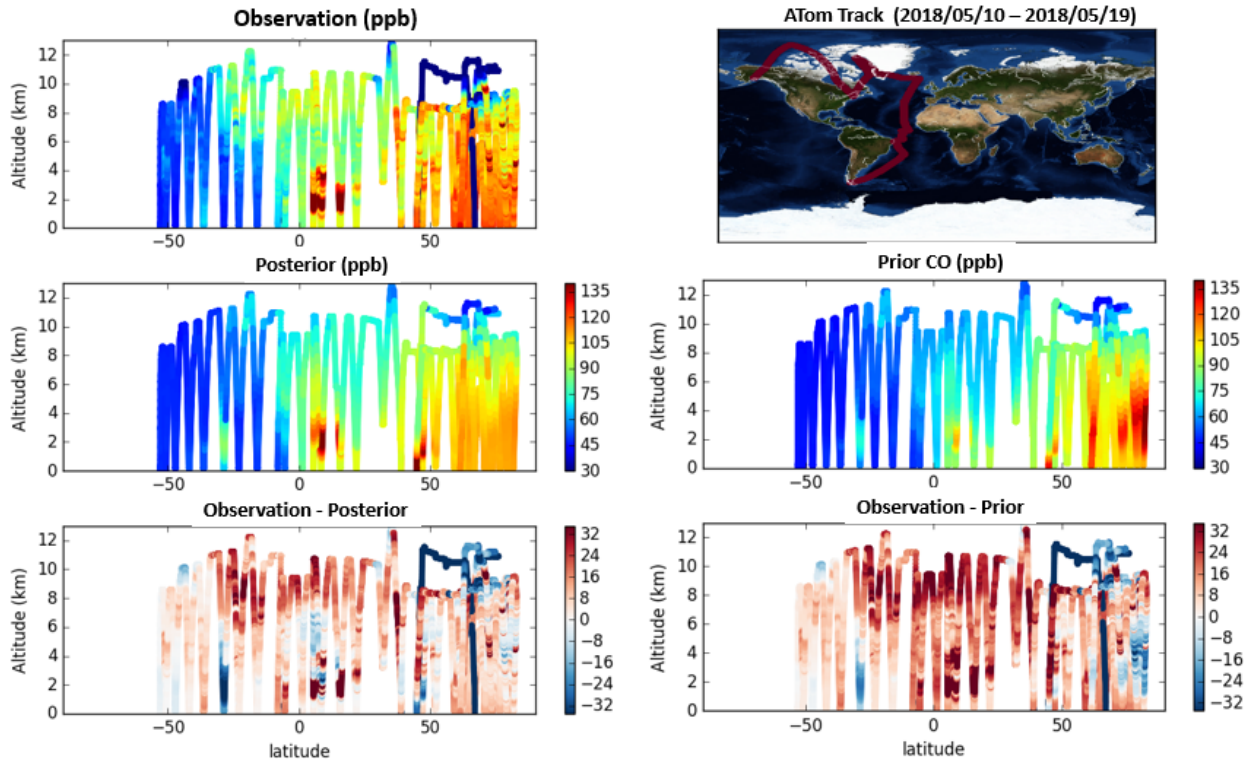
414



415  
 416 **Figure 4.** Model surface-PM2.5 a) annual mean averaged over two-decades (2002-2019), b)  
 417 change (second decade – first decade) between the first decade (2002-2009) and the second  
 418 decade (2010-2019), (c) comparison of the annual trend in four anthropogenic regions (Figure  
 419 1.d) , (d) comparison of the annual trend in four wild fire dominated regions (Figure 1.d).  
 420



421  
 422 **Figure 5.** Comparison of the monthly surface CO concentration between surface flask  
 423 measurements, model surface concentration simulated with the prior CO emission (prior), and  
 424 model surface concentration simulated with MOPITT-CO constrained CO emission (posterior).  
 425 These four regions were chosen as they were the only sites that provide a complete record over  
 426 the study period.  
 427

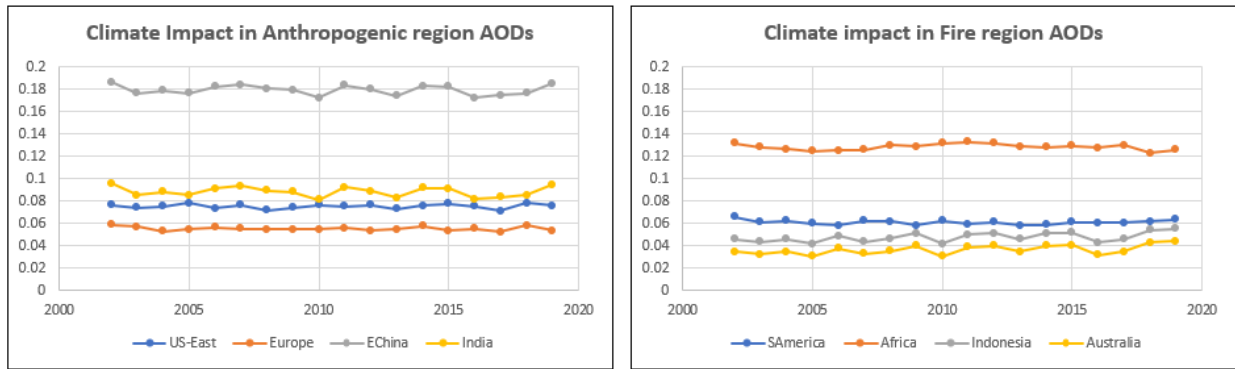


429

430 **Figure 6.** Comparison of the profile CO concentration between the aircraft measurements from  
 431 NASA’s Atmospheric Tomography Mission (ATom), model concentration profile simulated  
 432 with the prior CO emission (prior) and model concentration profile computed with the MOPITT-  
 433 CO constrained CO emission (posterior).

434

435  
436  
437



438  
439  
440  
441

**Figure 7.** Modeled AOD trends in four anthropogenic and four wildfire dominated regions for a constant emission scenario.

442 **References**

443

444 Andela, N. et al. (2017), A human-driven decline in global burned area, *Science*, 356, 1356–  
445 1362, doi:10.1126/science.aal4108.

446 Andreae, M. O., D. Rosenfeld, P. Artaxo, A. A. Costa, G. P. Frank, K. M. Longo, and M. Silva-  
447 Dias (2004), Smoking rain clouds over the Amazon, *Science*, 303(5662), 1337–1342.

448 Bauer, S. E., U. Im, K. Mezuman, and C. Y. Gao (2019), Desert Dust, Industrialization, and  
449 Agricultural Fires: Health Impacts of Outdoor Air Pollution in Africa, *Journal of*  
450 *Geophysical Research-Atmospheres*, 124(7), 4104–4120, doi:10.1029/2018JD029336.

451 Bennett, J. E., H. Tamura-Wicks, R. M. Parks, R. T. Burnett, C. A. Pope III, M. J. Bechle, J. D.  
452 Marshall, G. Danaei, and M. Ezzati (2019), Particulate matter air pollution and national and  
453 county life expectancy loss in the USA: A spatiotemporal analysis, *PLOS Medicine*, 16(7),  
454 e1002856, doi:10.1371/journal.pmed.1002856.

455 Bouwman, A.F., D. S. Lee, W. A. H. Asman, et al, A global high-resolution emission inventory  
456 for ammonia, *Global Biogeochemical Cycles*, Vol. 11, No. 4, 561-587, 1997

457 Buchholz, R. R., Worden, H. M., Park, M., et al., Air pollution trends measured from Terra: CO  
458 and AOD over industrial, fire-prone, and background regions, *Remote Sensing of*  
459 *Environment*, Accepted December 2020.

460 Burney, J. A. (2020), The downstream air pollution impacts of the transition from coal to natural  
461 gas in the United States, *Nature Sustainability*, 1–19, doi:10.1038/s41893-019-0453-5.

462 Byrne, B., Liu, J., Lee, M., Baker, I., Bowman, K. W., Deutscher, N. M., et al. (2020). Improved  
463 constraints on northern extratropical CO<sub>2</sub> fluxes obtained by combining surface-based and  
464 space-based atmospheric CO<sub>2</sub> measurements. *Journal of Geophysical Research:*  
465 *Atmospheres*, 125, e2019JD032029. <https://doi.org/10.1029/2019JD032029>

466 Dedoussi, I. C., S. D. Eastham, E. Monier, and S. R. H. Barrett (2020), Premature mortality  
467 related to United States cross-state air pollution, *Nature*, 1–19, doi:10.1038/s41586-020-  
468 1983-8.

469 Deeter, M. N., D. P. Edwards, G. L. Francis, J. C. Gille, D. Mao, S. Martinez-Alonso, H. M.  
470 Worden, D. Ziskin, and M. O. Andreae (2019), Radiance-based retrieval bias mitigation for the  
471 MOPITT instrument: the version 8 product, *Atmos. Meas. Tech.*, 12(8), 4561–4580,  
472 doi:[10.5194/amt-12-4561-2019](https://doi.org/10.5194/amt-12-4561-2019).

473

474 Dey, S., and L. Di Girolamo (2011), A decade of change in aerosol properties over the Indian  
475 subcontinent, *Geophys. Res. Lett.*, 38(14), n/a–n/a, doi:10.1029/2011GL048153.

476 DSc, D. A. J. C. et al. (2017), Estimates and 25-year trends of the global burden of disease  
477 attributable to ambient air pollution: an analysis of data from the Global Burden of Diseases  
478 Study 2015, *The Lancet*, 389(10082), 1907–1918, doi:10.1016/S0140-6736(17)30505-6.

479 Friedlingstein, P. et al. (2019), Global Carbon Budget 2019, *Earth Syst. Sci. Data*, 11(4), 1783–  
480 1838, doi:10.5194/essd-11-1783-2019.

481 Haywood, J. M., and V. Ramaswamy (1998), Global sensitivity studies of the direct radiative  
482 forcing due to anthropogenic sulfate and black carbon aerosols, *Journal of Geophysical*  
483 *Research: Atmospheres*, 103(D6), 6043–6058, doi:10.1029/97JD03426.

484 Henze, D. K., A. Hakami, and J. H. Seinfeld (2007), Development of the adjoint of GEOS-  
485 Chem, *Atmospheric Chemistry and Physics*, 7(9), 2413–2433.

486 Hilboll, A., A. Richter, and J. P. Burrows (2013), Long-term changes of tropospheric  
487 NO<sub>2</sub> over megacities derived from multiple satellite instruments,  
488 *Atmospheric Chemistry and Physics*, 13(8), 4145–4169, doi:10.5194/acp-13-4145-2013.

489 Huang, R.-J. et al. (2014), High secondary aerosol contribution to particulate pollution during  
490 haze events in China, *Nature*, 1–5, doi:10.1038/nature13774.

491 Jaeglé, L., P. K. Quinn, T. S. Bates, B. Alexander, and J. T. Lin (2011), Global distribution of  
492 sea salt aerosols: new constraints from in situ and remote sensing observations, *Atmospheric*  
493 *Chemistry and Physics*, *11*(7), 3137–3157, doi:10.5194/acp-11-3137-2011.

494 Jiang, J. H., H. Su, L. Huang, Y. Wang, S. Massie, Bin Zhao, A. Omar, and Z. Wang (2018),  
495 Contrasting effects on deep convective clouds by different types of aerosols, *Nat Commun*,  
496 1–7, doi:10.1038/s41467-018-06280-4.

497 Jiang, Z., D. B. A. Jones, H. M. Worden, M. N. Deeter, D. K. Henze, J. Worden, K. W.  
498 Bowman, C. A. M. Brenninkmeijer, and T. J. Schuck (2013), Impact of model errors in  
499 convective transport on CO source estimates inferred from MOPITT CO retrievals, *Journal*  
500 *of Geophysical Research-Atmospheres*, *118*(4), 2073–2083, doi:10.1002/jgrd.50216.

501 Jiang, Z., J. R. Worden, H. Worden, M. Deeter, D. B. A. Jones, A. F. Arellano, and D. K. Henze  
502 (2017), A 15-year record of CO emissions constrained by MOPITT CO observations,  
503 *Atmospheric Chemistry and Physics*, *17*(7), 4565–4583, doi:10.5194/acp-17-4565-2017-  
504 supplement.

505 Jimenez, J. L., M. R. Canagaratna, and N. M. Donahue (2009), Evolution of organic aerosols in  
506 the atmosphere, *science.sciencemag.org*, *326*, doi:10.1126/science.1179518.

507 Kahn, R. A., B. J. Gaitley, M. J. Garay, D. J. Diner, T. F. Eck, A. Smirnov, and B. N. Holben  
508 (2010), Multiangle Imaging SpectroRadiometer global aerosol product assessment by  
509 comparison with the Aerosol Robotic Network, *J. Geophys. Res.*, *115*(D23), D23209,  
510 doi:10.1029/2010JD014601.

511 Karplus, V. J., S. Zhang, and D. Almond (2018), Quantifying coal power plant responses to  
512 tighter SO<sub>2</sub> emissions standards in China, *Proceedings of the National Academy of Sciences*  
513 *of the United States of America*, *115*(27), 7004–7009, doi:10.1073/pnas.1800605115.

514 Kaufman, Y. J., I. Koren, L. A. Remer, D. Rosenfeld, and Y. Rudich (2005), The effect of  
515 smoke, dust, and pollution aerosol on shallow cloud development over the Atlantic Ocean,  
516 *Proceedings of the National Academy of Sciences of the United States of America*, *102*(32),  
517 11207–11212, doi:10.1073/pnas.0505191102.

518 Koren, I., O. Altaratz, L. A. Remer, G. Feingold, J. V. Martins, and R. H. Heiblum (2012),  
519 Aerosol-induced intensification of rain from the tropics to the mid-latitudes, *Nature*  
520 *Geoscience*, 5(2), 118–122, doi:10.1038/ngeo1364.

521 Krotkov, N. A. et al. (2016), Aura OMI observations of regional SO<sub>2</sub>  
522 and NO<sub>2</sub> pollution changes from 2005 to 2015, *Atmospheric*  
523 *Chemistry and Physics*, 16(7), 4605–4629, doi:10.5194/acp-16-4605-2016.

524 Kuhns, H., Green, M., and Etyemezian, V.: Big Bend Regional Aerosol and Visibility  
525 Observational (BRAVO) Study Emissions Inventory, Report prepared for BRAVO Steering  
526 Committee, Desert Research Institute, Las Vegas, Nevada, 2003.

527 Liao, H., D. K. Henze, J. H. Seinfeld, S. Wu, and L. J. Mickley (2007), Biogenic secondary  
528 organic aerosol over the United States: Comparison of climatological simulations with  
529 observations, *J. Geophys. Res.*, 112(D6), 13791–1, doi:10.1029/2006JD007813.

530 Liu, J. J., D. B. A. Jones, J. R. Worden, D. Noone, M. Parrington, and J. Kar (2009), Analysis of  
531 the summertime buildup of tropospheric ozone abundances over the Middle East and North  
532 Africa as observed by the Tropospheric Emission Spectrometer instrument, *J. Geophys. Res.*,  
533 114(D5), D05304, doi:10.1029/2008JD010993.

534 Lu, X., S. Zhang, J. Xing, Y. Wang, W. Chen, D. Ding, Y. Wu, S. Wang, L. Duan, and J. Hao  
535 (2020), Progress of Air Pollution Control in China and Its Challenges and Opportunities in  
536 the Ecological Civilization Era, *Engineering*, 1–9, doi:10.1016/j.eng.2020.03.014.

537 de Jesus, A. L. et al. (2020), Long-term trends in PM<sub>2.5</sub> mass and particle number  
538 concentrations in urban air: The impacts of mitigation measures and extreme events due to  
539 changing climates, *Environmental Pollution*, 263(Part A), 114500,  
540 doi:10.1016/j.envpol.2020.114500.

541 Mehta, M., R. Singh, A. Singh, N. Singh, Anshumali (2016), Recent global aerosol optical depth  
542 variations and trends — A comparative study using MODIS and MISR level 3 datasets,  
543 *Remote Sensing of Environment*, 181(C), 137–150, doi:10.1016/j.rse.2016.04.004.

544 Metzger, S., Dentener, F., Pandis, S., and Lelieveld, J (2002), Gas/aerosol partitioning: 1. A  
545 computationally efficient model, *J. Geophys. Res.-Atmos.*, 107, 4312,  
546 doi:10.1029/2001JD001102.

547 Miyazaki, K., Eskes, H., Sudo, K., Boersma, K. F., Bowman, K., and Kanaya, Y.: Decadal  
548 changes in global surface NO<sub>x</sub> emissions from multi-constituent satellite data assimilation,  
549 *Atmos. Chem. Phys.*, 17, 807–837, <https://doi.org/10.5194/acp-17-807-2017>, 2017.

550 Olivier, J. G. J. and Berdowski, J. J. M.: Global emissions sources and sinks, in: *The Climate*  
551 *System*, edited by: Berdowski, J., Guicherit, R., and Heij, B. J., A. A. Balkema  
552 Publishers/Swets & Zeitlinger Publishers, Lisse, the Netherlands, 33–78, 2001

553 Ramanathan, V. et al. (2001), Indian Ocean Experiment: An integrated analysis of the climate  
554 forcing and effects of the great Indo-Asian haze, *Journal of Geophysical Research-*  
555 *Atmospheres*, 106(D22), 28371–28398, doi:10.1029/2001JD900133.

556 Ramanathan, V., C. Chung, D. Kim, T. Bettge, L. Buja, J. T. Kiehl, W. M. Washington, Q. Fu,  
557 D. R. Sikka, and M. Wild (2005), Atmospheric brown clouds: Impacts on South Asian  
558 climate and hydrological cycle, *Proceedings of the National Academy of Sciences of the*  
559 *United States of America*, 102(15), 5326–5333, doi:10.1073/pnas.0500656102.

560 Roberts, G. C., M. O. Andreae, W. Maenhaut, and M. T. Fernandez-Jimenez (2001),  
561 Composition and sources of aerosol in a central African rain forest during the dry season, *J.*  
562 *Geophys. Res.*, 106(D13), 14423–14434, doi:10.1029/2000JD900774.

563 Rosenfeld, D. et al. (2014), Global observations of aerosol-cloud-precipitation-climate  
564 interactions, *Rev. Geophys.*, 52(4), 750–808, doi:10.1175/1520-  
565 0493(1994)122<1837:DCCSIT>2.0.CO;2.

566 Saleh, R. et al. (2014), Brownness of organics in aerosols from biomass burning linked to their  
567 black carbon content, *Nature Geoscience*, 7(9), 647–650, doi:10.5194/acp-11-7669-2011.

568 Satheesh, S. K., and V. Ramanathan (2000), Large differences in tropical aerosol forcing at the  
569 top of the atmosphere and Earth's surface, *Nature*, 405(6782), 60–63.

570 Sato, Y., D. Goto, T. Michibata, K. Suzuki, T. Takemura, H. Tomita, and T. Nakajima (2018),  
571 Aerosol effects on cloud water amounts were successfully simulated by a global cloud-  
572 system resolving model, *Nat Commun*, 9(1), 1227, doi:10.1256/qj.03.187.

573 Science, N. M., 2011 (2011), Aerosol indirect effect on biogeochemical cycles and climate,  
574 *science.sciencemag.org*, 334, doi:10.1126/science.1207374.

575 Seinfeld, J. H. et al. (2016), Improving our fundamental understanding of the role of  
576 aerosol–cloud interactions in the climate system, *Proceedings of the National Academy of*  
577 *Sciences of the United States of America*, 113(21), 5781–5790,  
578 doi:10.1073/pnas.1514043113.

579 Streets, D. G., Y. Wu, and M. Chin (2006), Two-decadal aerosol trends as a likely explanation of  
580 the global dimming/brightening transition, *Geophys. Res. Lett*, 33(15), L17802–25,  
581 doi:10.1029/2006GL026471.

582 Streets, D., Zhang, Q., Wang, L., He, K., Hao, J., Wu, Y., Tang, Y., and Carmichael, G.:  
583 Revisiting China’s CO emissions after the Transport and Chemical Evolution over the  
584 Pacific (TRACE-P) mission: Synthesis of inventories, atmospheric modeling, and  
585 observations, *J. Geophys. Res.-Atmos.*, 111, D14306, doi:10.1029/2006JD007118,  
586 2006.T.C. Bond et al. Historical emissions of black and organic carbon aerosol from energy-  
587 related combustion, 1850-2000, *Global Biogeochemical Cycles*, 21 GB2018, doi:  
588 10.1029/2006GB002840, 2007

589 Van Damme, M., L. Clarisse, S. Whitburn, J. Hadji-Lazaro, D. Hurtmans, C. Clerbaux, and P.-F.  
590 X. O. Coheur (2018), Industrial and agricultural ammonia point sources exposed, *Nature*, 1–  
591 12, doi:10.1038/s41586-018-0747-1.

592 van der Werf, G. R. et al. (2017), Global fire emissions estimates during 1997–2016, *Earth Syst.*  
593 *Sci. Data*, 9(2), 697–720, doi:10.5194/acp-9-5785-2009.

594 van der Werf, G. R., Randerson, J. T., Giglio, L., van Leeuwen, T. T., Chen, Y., Rogers, B. M.,  
595 Mu, M., van Marle, M. J. E., Morton, D. C., Collatz, G. J., Yokelson, R. J., and Kasibhatla,

596 P. S. (2017). Global fire emissions estimated during 1997–2016. *Earth Syst. Sci. Data*,  
597 9(2):697–720.

598 van der Werf, G. R., J. T. Randerson, L. Giglio, G. J. Collatz, M. Mu, P. S. Kasibhatla, D. C.  
599 Morton, R. S. Defries, Y. Jin, and T. T. van Leeuwen (2010), Global fire emissions and the  
600 contribution of deforestation, savanna, forest, agricultural, and peat fires (1997–2009),  
601 *Atmospheric Chemistry and Physics*, 10(23), 11707–11735, doi:10.5194/acp-10-11707-  
602 2010.

603 van Donkelaar, A., R. V. Martin, M. Brauer, and B. L. Boys (2015), Use of Satellite  
604 Observations for Long-Term Exposure Assessment of Global Concentrations of Fine  
605 Particulate Matter, *Environmental Health Perspectives*, 123(2), 135–143,  
606 doi:10.1289/ehp.1408646.

607 Vestreng, V. and Klein, H.: Emission data reported to UNECE/EMEP, Quality assurance and  
608 trend analysis Presentation of WebDab, Norwegian Meteorological Institute ,Oslo, Norway,  
609 MSC-W Status Report, 2002.

610 Warner, J. X., R. R. Dickerson, Z. Wei, L. L. Strow, Y. Wang, and Q. Liang (2017), Increased  
611 atmospheric ammonia over the world's major agricultural areas detected from space,  
612 *Geophys. Res. Lett*, 44(6), 2875–2884, doi:10.1002/2016GL072305.

613 Worden, H. M., A. A. Bloom, J. R. Worden, Z. Jiang, E. A. Marais, T. Stavrou, B. Gaubert,  
614 and F. Lacey (2019), New constraints on biogenic emissions using satellite-based estimates  
615 of carbon monoxide fluxes, *Atmospheric Chemistry and Physics*, 19(21), 13569–13579,  
616 doi:10.5194/acp-19-13569-2019.

617 Worden, J. et al. (2009), Observed vertical distribution of tropospheric ozone during the Asian  
618 summertime monsoon, *J. Geophys. Res*, 114(D13), D13304, doi:10.1029/2008JD010560.

619 Worden, J. R., A. A. Bloom, S. Pandey, Z. Jiang, H. M. Worden, T. W. Walker, S. Houweling,  
620 and T. Röckmann (2017), Reduced biomass burning emissions reconcile conflicting  
621 estimates of the post-2006 atmospheric methane budget, *Nat Commun*, 1–11,  
622 doi:10.1038/s41467-017-02246-0.

623 Yin, Y., F. Chevallier, P. Ciais, G. Broquet, A. Fortems-Cheiney, I. Pison, and M. Saunois  
624 (2015), Decadal trends in global CO emissions as seen by MOPITT, *Atmospheric Chemistry  
625 and Physics*, 15(23), 13433–13451, doi:10.5194/acp-15-13433-2015.

626 Zhao, B., J. H. Jiang, Y. Gu, D. Diner, J. R. Worden, K. N. Liou, S. HH, X. J, M. J. Garay, and  
627 L. Huang (2017), Decadal-scale trends in regional aerosol particle properties and their  
628 linkage to emission changes, *Environ. Res. Lett.*, doi:10.1088/1748-9326.

629